EXAMINING THE RELATIONSHIP BETWEEN WIND TURBINE BLADE PERFORMANCE AND TIP VORTEX BEHAVIOUR IN THE WAKE

J. WHALE

Department of Mechanical Engineering, The University of Edinburgh

The King's Buildings, Edinburgh, EH9 3JL, Scotland

SYNOPSIS : This paper details the results of laboratory tests on a model wind turbine rotor at the University of Edinburgh and examines tip vortex behaviour which questions the assumptions of current rotor performance prediction codes. Results are compared with wind-tunnel data from the Technical University of Delft and simulations from a vortex wake code developed at the University of Stuttgart. A Biot-Savart calculation is undertaken to provide insight into how the observed tip vortex effects may affect the calculation of performance of a wind turbine rotor.

NOTATION

t	time	s
R	blade radius	m
c	blade chord	m
z	axial distance from rotor	m
x	radial distance from hub	m
α	angle of attack	deg.
Ω	blade angular velocity	rad/s
V_o	freestream velocity	m/s
W	relative velocity at blade	m/s
w	induced velocity at blade	m/s
ς	vorticity	s-1
p	pitch of helical tip vortex	m
Γ	vortex strength	m^2/s
Γ_t	vortex strength at tip	m^2/s
Γ_{mod}	modified vortex strength: $\Gamma.(x/R)$	m^2/s
Γ_{max}	maximum bound circulation	m^2/s
ν	kinematic viscosity	m^2/s
λ	tip speed ratio: $\Omega R/V_o$	–
Re	Reynolds number: Wc/ν	–
C_L	lift coefficient	–
	normalisation factors :	
t_o	time: $\pi R/\lambda V_o$	s
ς_o	vorticity: $3c/V_o$	s-1
Γ_o	circulation: $2\pi V_o c$	m^2/s

1 INTRODUCTION

The discrepancy between theoretical predictions of horizontal-axis wind turbine (HAWT) performance and experimental measurements has been the subject of examination for some time. Various performance prediction codes have been developed which can be classified by their approach to modelling the relationship between the wake structure and the induced velocities (and hence forces) at points on the blade. For design purposes, it is essential to predict blade loads accurately, to estimate rotor power output and structural stresses.

The most common performance prediction codes currently used in HAWT design are based on blade/element momentum theory (BEMT). The theory has proved to be deficient in situations where high blockage exists (low windspeeds) or where the rotor is wholly or partially stalled (high windspeeds). Vortex wake models (induction models) represent an attempt to calculate a more realistic representation of the wake, consistent with the notion of helical vortex filaments shed from the trailing edge of the blade and convected downstream at wake velocity. Induction models, however, have provided no significant gain in accuracy with respect to

increase in computational time and to date, HAWT designers have not found a vortex wake code that is preferred to BEMT techniques.

Both BEMT and vortex wake codes are modelled on the premise that there is no exchange of flow between the freestream and the wake. Thus, conservation of mass leads us to expect an expanding wake with an asymptotic decrease in tip vortex pitch with downstream distance. In addition, most codes are based on potential flow theory and neglect the influence of viscous effects. These assumptions dictate the geometry and strength of the trailing helical vortex shed from a turbine blade and thus govern the calculation of the induced velocities at the blade.

There is growing evidence to suggest that the assumptions of current theory do not accurately describe the helical vortex system in the wake. In wind-tunnel smoke studies at FFA in Sweden, Dahlberg and Alfredsson[1], observed the slowdown of the wake as a temporary phenomenon behind the rotor and further downstream the tip vortex pitch was seen to increase. Montgomerie[2] attributed this wake acceleration to mixing of the freestream. Smoke studies on full-scale turbines at Risoe in Denmark[3] revealed that the strength of tip vortices were affected by vortex coalescence at high tip speed ratios due to the short distance between them. In more recent experiments at the Technical University of Delft, L.J. Vermeer[4] found that the tip vortex velocity was not the average of flow outside and inside wake as predicted by BEMT.

At the University of Edinburgh, detailed measurements of the flow around laboratory-scale wind turbines have been recorded using the laser-optics technique of Particle Image Velocimetry (PIV). A preliminary analysis of tip vortex behaviour was undertaken, identifying positions of tip vortices by using the point of maximum vorticity in a region of flow around the tip vortex[5]. This was a crude approach but the observed tip vortex effects supported the view that the assumptions of BEMT are inadequate to accurately describe the wake of a wind turbine.

The aim of this paper is to provide an insight into how the observed wake effects may affect the calculation of performance of a wind turbine rotor. The paper details a more rigorous approach to calculating vortex strength and geometry from the measurements of the wake of the turbine model at Edinburgh. Results are compared with wind-tunnel data from Delft[4] and the results of simulations from a vortex wake code developed at the University of Stuttgart[10]. A simple semi-infinite straight-line vortex model is used to estimate the effect of tip vortex behaviour in the near wake on the calculation of induced velocity at the rotor.

2 PIV EXPERIMENTS

Detailed velocity and vorticity measurements were analysed from PIV experiments on a 2-blade wind turbine model with a flat-plate rotor of 175mm diameter and 10mm tip chord[6]. The experiments were conducted in an open water channel which was equipped with a recirculating current facility which allowed a steady flow velocity to be established in the channel. The model turbine was powered by an electric motor with closed loop speed control. A position encoder was used to record blade azimuthal angle. The motor speed was altered to achieve the desired tip speed ratio (λ). Tests were run for tip speed ratios in the range $\lambda = 3-8$, corresponding to tip chord Reynolds numbers of 6,500~16,000.

The flow in the near wake was seeded with conifer pollen and a two-dimensional cross-section of the wake was illuminated by a scanning laser beam[7]. Multiple-exposed photographs of the illuminated flow regions produced flow records of the pollen particles which could be analysed to find the spacing between the particle images and hence the local flow velocity. This is the basis of the PIV technique which allows complete 2-d vector flow fields to be captured at a single instant and in recent years has developed into a powerful tool for flow visualisation and measurement.

Applying the PIV technique produced maps of detailed velocity vectors in the wake of the

model turbine. Averaging instantaneous PIV records at one blade azimuthal angle extracts the coherent structure of a 2-d cross-section of the trailing vortex spiral from the superposed turbulence. The averaged PIV velocity vector maps were used to calculate contour plots of vorticity which formed the basis for all subsequent analysis.

3 RESULTS

3.1 Tip vortex behaviour in the PIV experiments

Figure 1 shows a typical vorticity contour plot of the flow in the lower half of the near wake of the two-bladed flat-plate model operating at a tip speed ratio of λ=6. The blade is featured in the top left hand corner of the plot. The contours of the maps join points of equal vorticity with vortex strengths represented by varying degrees of lightness.

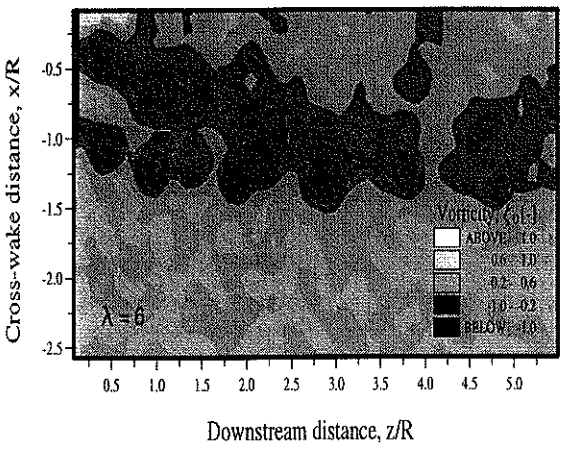

Figure 1 PIV vorticity contour plot of lower half of wake at λ = 6

The tip vortices are clearly shown in addition to a section of inboard vorticity which moves under the influence of wake expansion to merge with the tip vortex spiral at around 2*R* downstream. The merger appears to induce unstable behaviour in the tip vortex system. At *z/R*=2, the tip vortex catches up with the preceding vortex which rolls over the top of its neighbour by *z/R*=3. This pairing process has been commented upon previously in full-scale smoke studies[3].

The inboard region of vorticity is independent of the root vortices, which are of opposite sign and appear to dissipate within one blade revolution. The origin of the inboard vorticity is discussed in section 4.1.

The strength and location of the trailing tip vortices are calculated, for each λ. The contour plots allow a value of 'background' vorticity to be chosen which discriminates between vorticity due to tip vorticity and vorticity due to inboard vorticity and turbulence. Dividing a region of flow containing the tip vortex into discrete elements, the strength of each tip vortex is calculated by summation of all elements with a value of vorticity greater than the background value. The strength of each element, weighted by its position in the wake and divided by the total strength of the elements yields an axial and radial position for the centroid of the vortex.

3.2 Tip vortex strength

Figure 2 shows a plot of tip vortex strength versus axial distance downstream of the rotor for λ=2–6. Values of modified vortex strength, $\Gamma_{mod} = \Gamma(x/R)$ are plotted to account for the effect of thinning of vortex filaments due to wake expansion.

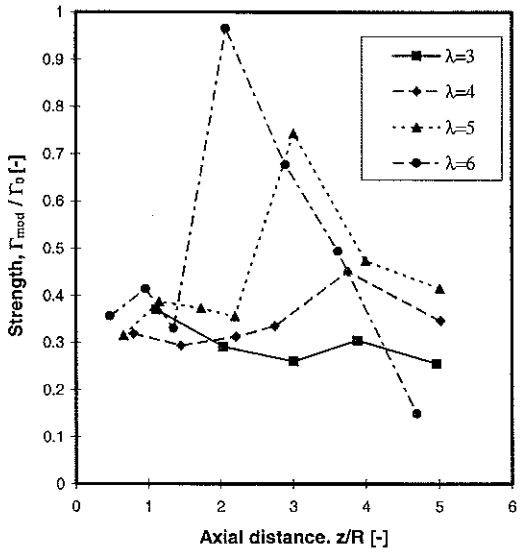

Figure 2 Strength of tip vortices with downstream distance

The curves in Figure 2 show a general trend of increased vortex strength with increased tip speed. This is to be expected since at higher tip speeds greater turbulence in the wake will preserve the energy in the tip vortex system. Less expected, is the increase in strength of the 4th or 5th vortex downstream (in the region $2<z/R<4$) for each tip speed ratio. It is noted that as λ increases, the increase in vortex strength is greater and appears closer to the rotor plane.

At λ=5 and λ=6, the large increase in vortex strength is likely to be due to vortex coalescence between adjacent tip vortices (see Figure 1). A decrease in tip vortex spacing with increased λ is likely to cause the pairing to occur closer to the rotor for higher tip speed ratios. The rapid decay of the case λ=6 shows the interaction may be ultimately destructive. A closer look at the vorticity contour plots for lower tip speed ratios of λ=3 and λ=4 suggests that, although there is no pairing of tip vortices, vorticity from the inner wake may 'feed' the tip vortex system and produce the increase of strength around z/R=4 seen in Figure 2. Moving under the influence of wake expansion, the section of inboard vorticity would be expected to interact with the tip vortex system closer to the rotor plane as λ increases.

3.3 Tip vortex geometry

Obtaining information about the axial position of the centroid of each tip vortex allows insight into the pitch and changes in the pitch of the trailing vortex spiral. In Figure 3, the average pitch of the helical vortex is plotted for various tip speed ratios.

The figure considers three sections of the wake; up to $2R$ behind the rotor, between $2-4R$ and greater than $4R$ downstream. For $z/R<2$, the graph shows a decrease in the average spiral pitch with increased λ and is consistent with a 'packing' of the vortex spiral behind the rotor with increased blade passing frequency. A similar trend is observed for the region between $2<z/R<4$; the vortex instability present in this region (see section 3.1) may explain the increase in scatter in the data.

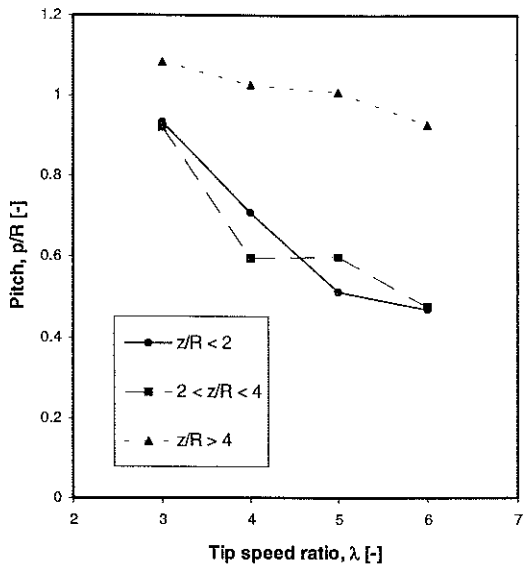

Figure 3 Average pitch of the trailing vortex spiral

For $z/R>4$, the graph shows a dramatic increase in the average pitch with values around $1R$ for each λ. This is contrary to the assumptions of both BEMT and induction theories which predict an asymptotic decrease in tip vortex pitch with axial distance downstream. For the cases λ=5 and λ=6 this corresponds to approximately twice the pitch of the spiral in the section of wake less than $4R$ from the rotor. Thus, vortex coalescence would seem a likely explanation for the increased vortex pitch. The lack of tip vortex interaction for λ=3 and λ=4, on the other hand, provide evidence that, at least in these cases, the tip vortex spiral is 'uncoiling'. It is plausible that (as suggested by Montgomerie[3]) there is a mixing of the freestream and the wake at around z/R=4 which provides a wake acceleration and increases the pitch of the tip vortex spiral.

Information about the radial position of the tip vortices yields an impression of the shape of the wake boundary. Figure 4 plots the radial position against axial position of the tip vortices for each tip speed ratio case. The data for λ=6 is correctly positioned on the plot while, for clarity, the remaining curves are offset from their true values by multiples of 0.25.

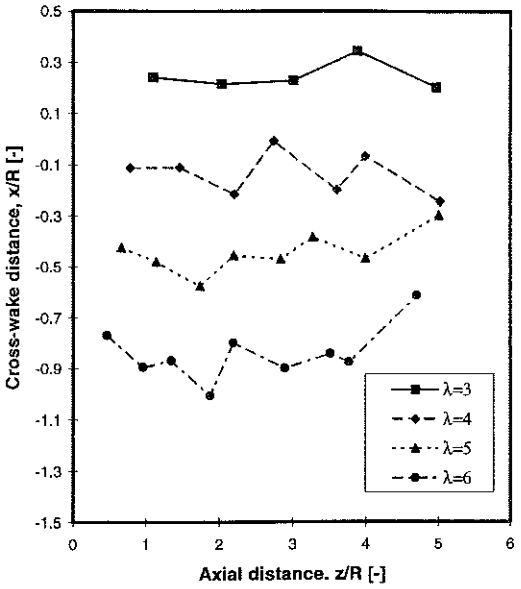

Figure 4 The shape of the wake boundary

The shape of the wake boundary suggests that, as in the previous graph, the figure can be examined in terms of three regions in the wake. Up to $2R$ behind the rotor, the wake behaves as predicted by current theory; the shape of the wake shows an expansion which increases as λ increases. The scatter of data in the region between $2-4R$ confirms this section of the wake to be influenced by vortex instability. The graphs show that this instability in tip vortex position appears to correlate with an initial decrease in radial position, suggesting the influence of tip vortex interaction either with each other (pairing) or with the inner wake vorticity as proposed in section 3.1.

At downstream distances greater than $4R$, the graph shows that low λ cases continue to exhibit wake expansion but the cases of λ=5 and λ=6 exhibit a marked contraction of the wake. This suggests that wake speed-up also occurs at higher λ and it is plausible that it is caused by an exchange of momentum between the freestream and wake, as mentioned above. Marked contraction of the downstream wake is characteristic of a turbulent wake state, as defined in Eggleston and Goddard[8], and is overlooked by BEMT.

3.4 Comparison with wind-tunnel data and vortex wake code simulations

The Edinburgh data was compared with measurements from wind-tunnel studies at the Technical University of Delft[4,9] and with simulations from a vortex wake model developed at the University of Stuttgart[10].

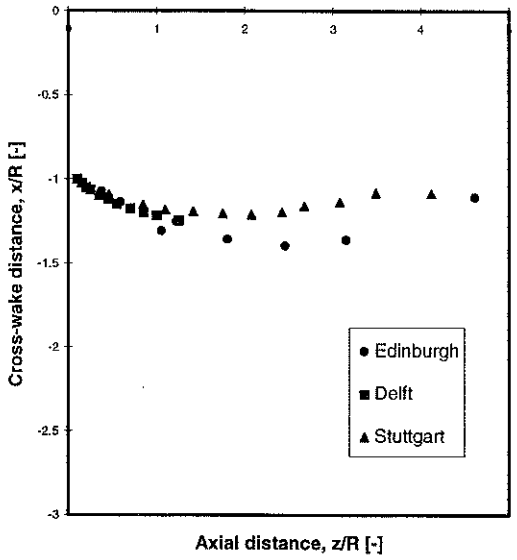

Figure 5 Comparison of the shape of the wake boundary at $\lambda = 8$

The TUDelft experiments involved detection of the passage of tip vortices behind a 2-blade, 1.2m diameter rotor in an open jet wind-tunnel using hot-wire equipment. Data from the wind-tunnel experiments were selected which were most suitable for comparison with the operating conditions of the Edinburgh tests. At the University of Stuttgart, a sophisticated vortex panel code has been developed which simulates the effects of vortex shedding and is able to predict the geometry and strength of vorticity on the rotor blades and in the wake. The code was run specifically to simulate the Edinburgh experiments[6].

In Figure 5, the shape of the wake boundary is compared for the case λ=8. The Edinburgh, Delft and Stuttgart measurements are in good agreement in terms of wake shape up to $1R$ downstream. For z/R>1, a large expansion of the wake is noted in the case of the Edinburgh data. At around z/R=2.5, the Edinburgh and

Stuttgart results both show signs of wake contraction.

Figure 6 compares the expansion of the wake at $1R$ downstream for the three sets of data over a range of tip speed ratios. The data shows a general increase in wake radius with tip speed ratio as expected. At low tip speed ratios there is very good agreement between the code and both sets of experimental results. For $\lambda>6$, the Edinburgh results show large wake expansion and the code has more success in predicting the wind-tunnel results.

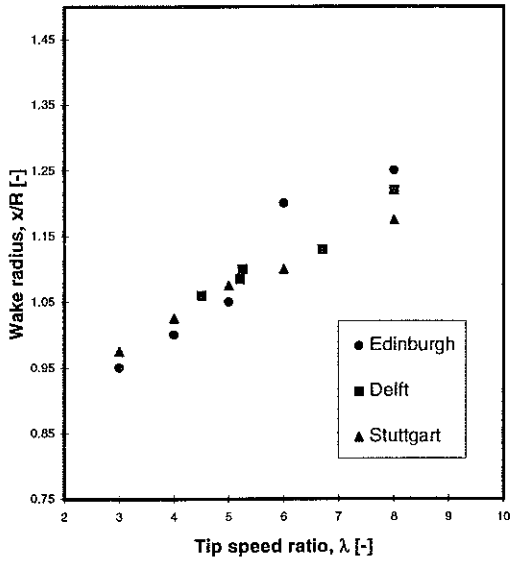

Figure 6 Comparison of the wake radius at 1R downstream

In the Delft hot-wire experiments, times were recorded for the tip vortex to travel specific distances. For the purposes of comparison, the vorticity contour plots of the Edinburgh and Stuttgart data were analysed as the progress of a single tip vortex. Times were normalised by the time between shedding of successive turns of the vortex spiral, t_o. Figure 7 plots the axial downstream position of the tip vortex versus time for the case $\lambda=8$. The slope of the data points yields the tip vortex velocity. The graph shows very good agreement between the experimental and theoretical data, up to $1R$ downstream. For $z/R>1$ there is a dramatic acceleration of the tip vortex in the case of the Edinburgh data while the Stuttgart data shows an increase in tip vortex velocity for $z/R>4$.

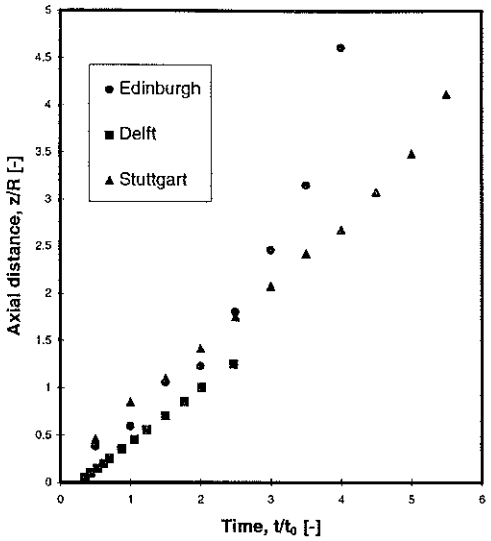

Figure 7 Comparison of tip vortex velocities in the wake at $\lambda = 8$

4 TIP VORTEX BEHAVIOUR AND BLADE PERFORMANCE

4.1 Tip vortex behaviour and blade-bound circulation

In order to correlate the observed tip vortex behaviour with blade performance, the PIV images were re-analysed on a finer grid scale in order to highlight the region of flow close to the blade. Figure 8 shows the result of re-analysing the data of Figure 1. The hub and part of the nacelle of the rig are seen in the top right hand corner of the plot. Figure 8 shows the contours of the tip and root vortices as well as a region of concentrated vorticity forming at approximately $z/R=0.2$, $x/R=-0.4$. It is possible that this is the start of the inner wake vorticity seen in Figure 1. Although the mechanism of its generation requires further investigation, the PIV results suggest that the inboard vorticity has its origins in changes in wake structure rather than the shedding of vorticity from the blade or nacelle. One possibility is that the inboard vorticity may be due to a velocity shear layer between the slow-moving wake core and the fast outer wake. The idea of a shear layer has some support in the reports of stretching of smoke filaments, inboard of the tip, in experiments by Pedersen and Antoniou[3].

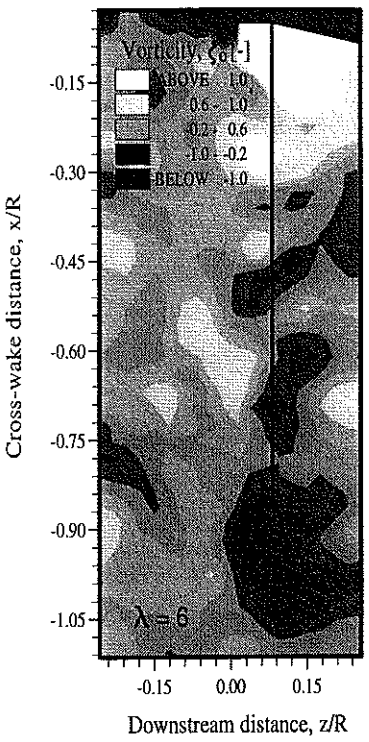

Figure 8 PIV vorticity contour plot of the flow at the rotor plane for λ=6

The vorticity data of Figure 8 is used to determine the strength of trailing vorticity at stations along the span of the blade and input into a lifting-line calculation. Figure 9 shows the result of the calculations, in terms of spanwise distributions of lift and angle of attack, for λ=6. The blade appears to experience stall for angles greater than 10°; a larger region of separated flow along the blade than would be expected at full-scale. This result is consistent with the low Reynolds numbers of the Edinburgh experiments. The values of the lift coefficients, however, are higher than expected for the low Re tests. The considerations of low Reynolds number experiments are further discussed in section 5.2.

Repeating the lifting-line calculations over a range of tip speed ratios, the spanwise circulation distribution is obtained in each case. In Figure 10, the strength of the shed vortex at $1R$ downstream is plotted as a function of maximum blade-bound circulation. Data from the wind-tunnel tests at TUDelft is used for comparison.

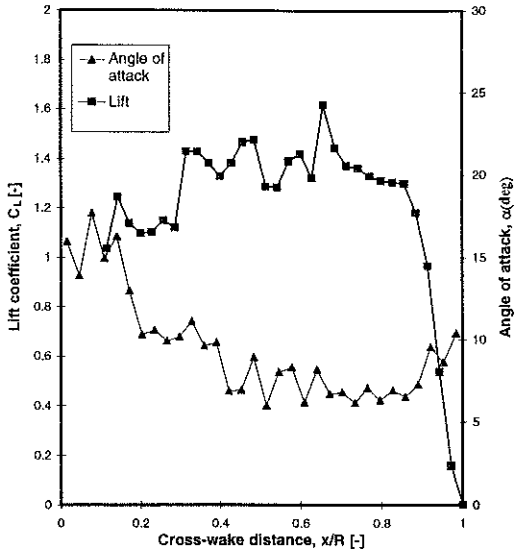

Figure 9 Spanwise distributions of lift and angle of attack on blade at λ = 6

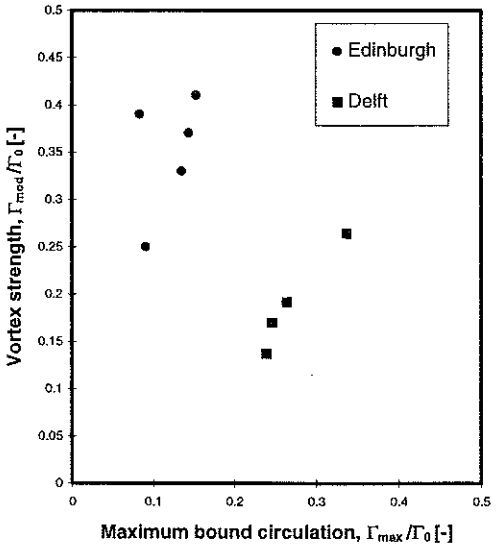

Figure 10 Comparing strength of shed vortex at 1R downstream

Both sets of data indicate a strong relationship between shed vorticity and maximum bound circulation on the blade. The comparatively high vortex strengths in the Edinburgh data may be a result of large vortices due to early separation on the blade in the low Reynolds number tests. In addition the lack of data very close to the blade in the PIV experiments may explain the low values of bound circulation compared to the wind-tunnel data.

4.2 Tip vortex behaviour and induced velocity at the blade

In order to gain a quantitative estimate of how the observed tip vortex behaviour may influence the calculation of blade performance, a simple Biot-Savart calculation was undertaken to examine the influence of the behaviour of the tip vortex spiral on the computation of induced velocity.

The near wake was modelled by a series of semi-infinite straight line vortices, separated by an axial distance, aR. Assuming the size of the vortices are O(c) and decay exponentially on a timescale of O(c^2/ν), the induced velocity at the blade tip can be shown to be

$$w = \frac{\Gamma_t(1-e^{-q})}{4\pi R}\sum_{n=1}^{\infty}\left[\frac{1}{p}+\frac{1}{\sqrt{(p^2+4)}}\right] \quad 1.$$

where $p = na$, $q = \frac{c^2}{4\pi\nu}$, Γ_t is the vortex strength at the tip, R and c are the radius and chord of the blade respectively and ν is the viscosity of the fluid.

The Biot-Savart calculations were carried out using eqn 1. to assess the effect of two tip vortex phenomena; the increase in pitch of the tip vortices at downstream distances greater than $2R$ and the increase in tip vortex strengths due to vortex interaction at $2-4R$ downstream. The changes in induced velocity due to these two effects were recorded as approximate estimates. In the case of λ=6, the results showed that the increase in pitch caused an 5% reduction in induced velocity at the tip and an increase in tip vortex strengths between $2-4R$ downstream caused an 25% increase in the induced velocity. In the latter case, the high factor may be partly due to the fact that the wake is very turbulent at this tip speed ratio. For the case λ=5, a tip speed ratio more pertinent to full-scale operation, the increase in pitch again resulted in an 5% decrease in induced velocity and vortex instability around $2-4R$ causes an 10% increase in induced velocity.

5 DISCUSSION

5.1 Comparison with previous experiments

The results of the Edinburgh tests confirm the increase in tip vortex pitch with downstream distance as suggested by Dahlberg and Alfredsson[1]. The reduction of induced velocities by an increase in pitch of the tip vortex spiral was expected since the tip vortices are further away from the rotor. This results in higher forces on the rotor and could be a factor in explaining why current theories underpredict rotor performance.

In cases where there was no observable interaction between adjacent tip vortices, the increase in strength of tip vortices in the section of the wake 2<z/R<4, suggests that the inboard vorticity may move under the influence of wake expansion to 'feed' the tip vortex system. Full-scale smoke studies at Risoe[3], however, observed that the tip vortices appeared to be independent of vorticity shed inboards of the tip vortex system. It is possible that the large wake expansion observed in the Edinburgh data in Figure 5 is responsible for the merger of the inboard vorticity with the tip vortex system. This is discussed further in the next section.

5.2 Scale effect, and sources of error

The PIV experiments contain a number of sources of error, many of which can be treated as negligible. A study of the influence of the walls of the water channel on the flow past the model rotor produced an estimate of correction for blockage of 2.5%. The combined systematic error from the PIV technique contributed less than 3% error in velocity measurement and random errors were responsible for 1% error. Errors in velocity measurement were compounded during vorticity calculations. The maximum error in vorticity, however, was estimated as 6%.

The PIV experiments were not designed to capture detailed flow over the blades and as a result, analysis of the PIV records at the rotor plane produced areas of sparse data very close to the blade. The lifting-line calculations compound errors in vorticity measurements

along the blade and ideally a further set of PIV tests, focusing on the rotor plane, are required.

The Biot-Savart calculation was a simple method of estimating the effect of the observed tip vortex behaviour on the calculation of induced velocity. The effect of replacing a curved vortex with a series of straight semi-infinite straight vortex lines in the near wake can, however, be shown to be negligible[11].

In terms of extrapolating these results to a full-scale machine, the most important concern is that of scale effect. The blade Reynolds number of the PIV tests was lower than full-scale by a factor of 1000, in some cases, and, as Figure 9 suggests, it is likely that there is a difference in the phenomena of separation and reattachment at the model blade, compared to full-scale. It is unclear as to what extent the differences in blade flow are conveyed to the wake structure.

If the explanation of its origin is correct, the phenomenon of inboard vorticity would be highlighted at low Re, when the boundary layer on the blades would be relatively thick. Conversely, it would be less pronounced on a full-scale wind turbine. In addition, High drag on the rotor at low Re may be responsible for the large wake expansion (see Figure 5) causing interaction of inner wake vorticity with the tip vortex system. Wake expansion may not be as extreme at full-scale and it is unclear whether a merger of inboard vorticity and tip vortices would occur. Figure 7 suggests that low Reynolds tests may encourage faster wake acceleration. This needs to be investigated further and data from further downstream in the higher Reynolds number wind-tunnel tests at Delft is required.

Despite likely differences between the model tests and full-scale flow, particularly at the blade, the broader aspects of fluid flow patterns usually show much less change than the corresponding lift-coefficients over the same range of Reynolds numbers[12]. Although full-wake structures may differ from those observed at model scale, there is a strong possibility that they will share fundamental similarities. Analysis of the PIV results may therefore yield a fundamental understanding of the relationship between vortex structure in the wake and the performance of a wind turbine rotor.

6 CONCLUSIONS

Analysis of the wake of a model wind turbine using PIV measurements has revelaed tip vortex behaviour which contradicts some of the assumptions of current wake theory. Examining various tip speed ratios, λ=2-8, the PIV results indicate that the wake behaves as current prediction codes suggest up to a distance of $2R$ downstream. Past this distance, the wake displays behaviour which affects the strength and fundamental geometry of the tip vortex spiral and is not accounted for by current theory.

An increase in the pitch of the tip vortex spiral was observed from the Edinburgh data at $4R$ downstream, for each tip speed ratio. This may be due to wake acceleration caused by re-entrainment of the freestream with the wake. At λ=5, a Biot-Savart calculation estimates that the increase in pitch of the tip vortex spiral reduces the induced velocity at the tip of the blade by around 5%.

The PIV vorticity plots reveal an inboard region of vorticity which moves under the effect of wake expansion to merge with the tip vortex system. For $\lambda \leq 5$, this may be responsible for increasing the strength of the trailing tip vortices at around $2-4R$ downstream. At $\lambda > 5$, the merger may be responsible for inducing pairing of tip vortices leading to an increase in tip vortex strength. At λ=5, A Biot-Savart calculation estimates that the increase in strength of the vortex spiral around $2-4R$ increases the induced velocity at the tip of the blade by around 10%. It is possible that the coalescence of tip and inboard vorticity is restricted to low-Reynolds number flows where large wake expansion is responsible for the merger.

PIV results for tip vortex velocity and wake expansion compare well with the Delft and Stuttgart results in the case λ =8, at least up to $1R$ downstream. Evidence of a strong relationship between strength of shed vortex

and blade bound circulation is found in both the Edinburgh and Delft experiments.

7 ACKNOWLEDGEMENTS

The author is extremely grateful for the contributions to this paper by Nord-Jan Vermeer of the Technical University of Delft and Rainer Bareiss of the University of Stuttgart. This project is funded by the Engineering and Physical Sciences Research Council.

REFERENCES

[1] Alfredsson, P.H. & Dahlberg, J.A. 1979 A preliminary wind-tunnel study of windmill wake dispersion in various flow conditions. *Technical Note FFA (Sweden), UA-1499*, Part 7.

[2] Montgomerie, B. 1990 The need for more measurements, *Proceedings of the IEA Aerodynamics Symposium*, Rome, Italy.

[3] Pedersen, T.F. & Antoniou, I. 1989 Visualisation of flow through a stall-regulated wind turbine rotor. *Proceedings of the 1989 European Wind Energy Conference,* Glasgow, Scotland, 83-89.

[4] Vermeer, L.J. 1994 Measurements on the properties of the tip vortex of a rotor model. *Proceedings of the 5th European Wind Energy Association Conference and Exhibition*, Thessaloniki, Greece, 805-808.

[5] Whale, J. 1997 Investigating fundamental properties of wind turbine wake structure using particle image velocimetry, *Proceedings of the IEA Aerodynamics Symposium*, Edinburgh, Scotland.

[6] Whale, J., Bareiss, R., Wagner, S. & Anderson, C. G. 1996 The wake structure of a wind turbine - comparison between PIV measurements and free-wake calculations. *Proceedings of the 1996 European Union Wind Energy Conference*, Gothenburg, Sweden, 457-460

[7] Gray, C., Greated, C.A., McCluskey, D.R. & Easson, W.J. 1991 An analysis of the scanning beam PIV illumination system, *Journal of Physics: Measurement Science and Technology*, **2**: 717-24.

[8] Eggleston, D. M. & Stoddard, F. S. 1987 *Wind Turbine Engineering Design*, Chapter 1, pp 30-35, Van Nostrand Reinhold.

[9] Vermeer, L.J., Briaire, J.J. & Doorne, C. van 1995 How strong is a tip vortex? *Proceedings of the 17th British Wind Energy Association Conference and Exhibition*, 59-64

[10] R.Bareiss, S.Wagner, 1993 The free wake / hybrid code ROVLM - a tool for aerodynamic analysis of wind turbines, *Proceedings of the European Community Wind Energy Conference*, Travemünde, Germany, 424-427.

[11] Miller, R.H 1964 Rotor blade harmonic air loading, *Journal of Royal Aeronautical Society*, **68**(640): 217-229.

[12] Gould, R.W.F. 1968 Design of a low-speed water channel. *NPL AeroReport*, 2-3.